Metalurgi (2022) 2: 49 - 56

METALURGI
Majalah Ilmu dan Teknologi
p-ISSN 0126-3188 | e-ISSN 2443-3926
ejurnalmaterialmetalurgi.lipi.go.id

HARDNESS AND CORROSION BEHAVIOR OF Ti-20Cu-20Ni-20Mn-20Zn AS HIGH ENTROPY ALLOY AND TI-13Cu-9Ni-5Mn-5Zn FOR MARINE STRUCTURE APPLICATION

Muhammad Azhar Ariefkha Dani[a,*], Bonita Dilasari[a], Yudi Nugraha Thaha[b], Ika Kartika[b], Fendy Rokhmanto[b]

[a] Department of Metallurgical Engineering, Bandung Institute of Technology
Jl. Ganesha 10, Bandung, Indonesia 40132
[b] Research Center for Metallurgy, National Research and Innovation Agency
Management Building 720, B.J. Habibie Sains and Technology Area, Banten, Indonesia 15343
*E-mail: m.azhar.ariefkha.dani@gmail.com

Received: 23-03-2022, Revised: 19-07-2022, Accepted: 04-10-2022

Abstract

Beta titanium alloys and titanium high entropy alloys are promising candidates for marine structural applications. This study aims to compare Ti-20Cu-20Ni-20Mn-20Zn high entropy alloy and Ti-13Cu-9Ni-5Mn-5Zn beta titanium alloy on microstructure, mechanical properties, and corrosion behavior in a 3.5% NaCl solution. Ti-20Cu-20Ni-20Mn-20Zn and Ti-13Cu-9Ni-5Mn-5Zn were produced by powder metallurgy. In the experimental results, it was observed that Ti-20Cu-20Ni-20Mn-20Zn alloy, as a high entropy alloy, has a low hardness value of 190.658 HV and a high corrosion rate of 1.7992 mm/year. The Ti-13Cu-9Ni-5Mn-5Zn alloy as the beta-titanium alloy has a high hardness value of 430.736 HV and a low corrosion rate of 0.12121 mm/year. The results indicate that Ti-13Cu-9Ni-5Mn-5Zn has better corrosion resistance in 3.5% NaCl solution and hardness than Ti-20Cu-20Ni-20Mn-20Zn high entropy alloy.

Keywords: *Beta-titanium, high entropy alloys, powder metallurgy, corrosion, marine structure application*

1. INTRODUCTION

Since the 1950s, titanium alloys have been developed as structure materials for marine facilities, especially for ship hulls, marine power systems, and pipes. Marine titanium alloys mostly contain aluminum and molybdenum upon optimum doping with an adaptive strengthening of the hexagonal crystalline lattice (α-Ti). α-Ti is chosen because it has good weldability, which enables the production of large-size welded structures without additional thermal processing to remove residual welding stress [1]. However, α-Ti has low strength properties, is brittle, unable to heat treatment, and has a low forming ability [2].

Besides that, beta titanium (β-Ti) is one phase of titanium alloys that usually contains vanadium (V), molybdenum (Mo), niobium (Nb), and tantalum (Ta) [2]. It has been used in applications that demand high strength, good corrosion resistance, excellent biocompatibility, good ductility, good weldability, good stability at a temperature above 315 ºC, and ease of fabrication [2], [3]. Moreover, the β-Ti alloy has better formability and is easier to fabricate than the alpha phase titanium [2]. β-Ti alloys such as Ti-8Mn, Ti-45Nb, Ti-15Mo-5Zr, Ti-11.5Mo-6Zr-4.5Sn, and Ti-35V-15Cr have good corrosion resistance to Cl^- ions and show good corrosion resistance for marine applications [4]. β-Ti alloy properties provide significant advantages over other high-performance alloys. However, the main drawback of β-Ti alloys is their high cost due to increase raw materials cost [5].

On the other hand, high entropy alloys are currently of great research interest in materials science and engineering [6]. High entropy alloys are alloys designed to combine at least five essential elements in relatively high concentrations (5–35 at.%) compared to

DOI : 10.14203/metalurgi.v37i2.636

conventional alloys that have only one or two basic elements [6]–[11]. High entropy alloys have recently been developed due to their high strength properties, good corrosion resistance, and ease of fabrication [7], [12]. High entropy alloys recently being developed are Ti-Zr-Cu-Ni-Be alloy, 0.5Al-Co-Cr-Cu-Fe-Ni-0.2Ti alloy, Ta-Nb-Hf-Zr-Ti alloy, and Ta-Nb-V-Ti alloy [8]. To the best of our knowledge, there are still few studies on high entropy alloys using titanium in 2022, and no research on Ti-Cu-Ni-Mn-Zn high entropy alloy has been discovered.

The powder metallurgy method was used to create Ti-20Cu-20Ni-20Mn-20Zn high entropy alloy and Ti-13Cu-9Ni-5Mn-5Zn β-Ti alloy in the current work. Because of the uniform composition, metal savings, and lower processing costs, the powder metallurgy method was used for alloy production [13]. Copper (Cu), nickel (Ni), manganese (Mn), and zinc (Zn) are inexpensive alloying elements for the synthesis of beta titanium and high entropy alloy. Cu, Ni, and Mn are eutectoid elements forming beta-phase titanium [3]. Zinc (Zn) was selected to decrease the sintering temperature of the powder metallurgy process [14]. NaCl 3.5% is commonly used standard solution for marine corrosion simulation [1].

This study aims to compare the microstructure, mechanical properties, and corrosion behavior Ti-20Cu-20Ni-20Mn-20Zn high entropy alloy and Ti-13Cu-9Ni-5Mn-5Zn β-Ti alloy on their in a 3.5% NaCl solution for marine structure application.

2. MATERIALS AND METHODS

2.1 Materials

Powder metallurgy method was used to create Ti-20Cu-20Ni-20Mn-20Zn and Ti-13Cu-9Ni-5Mn-5Zn alloy compositions. Titanium, copper, nickel, manganese, and zinc (Merck, p.a grade) was precisely weighed and mixed for 5 minutes in mortar. It was then compacted for 30 seconds using Enerpac GP-105 at 500 MPa pressure to form a compact cylinder with a 1 cm diameter and 5 mm height. The compacted sample was sintered using GSL-1100X at 880 °C for 3 hours before being cooled to room temperature in an argon atmosphere in a quartz tube. The samples were polished on the Grinder Polisher-1B with water flowing through it using emery papers up to 2000 grit. This study used a Kroll solution consisting of 6 mL HNO3, 3 mL HF, and 100 mL H2O as the etching solution.

2.2 Characterization

The microstructure of Ti-20Cu-20Ni-20Mn-20Zn and Ti-13Cu-9Ni-5Mn-5Zn samples were characterized by JEOL JSM-6390A SEM-EDS (scanning electron microscope-energy dispersive spectroscopy).

Ti-20Cu-20Ni-20Mn-20Zn and Ti-13Cu-9Ni-5Mn5Zn alloys were investigated by Rigaku Smartlab XRD (x-ray diffraction) with Cu-Kα to identify the phase that was formed after the sintering process.

The Vickers Micro Hardness test was performed The Vickers Micro Hardness test was carried out at Mitutoyo AR Hardness with a loading of 0.3 KN and a loading speed of 12 seconds. The hardness test was carried out eight times on the surface of the specimen with a horizontally parallel pattern at Mitutoyo AR Hardness with a loading of 0.3 KN and a loading speed of 12 seconds. The hardness test was carried out eight times on the surface of the specimen with a horizontally parallel pattern.

Potentiodynamic polarization and EIS (electrochemical impedance spectroscopy) were used to investigate corrosion behavior in a 3.5% NaCl solution using a three-electrode system, with the samples serving as working electrodes, Ag/AgCl (KCl 1 M) serving as the reference electrode, and a platinum plate serving as the counter electrode. For marine environment simulation, a 3.5% NaCl solution at room temperature (25 °C) was used. Autolab 302 Multi BA was used to perform the electrochemical measurements. The potentiodynamic polarization was performed at a scan rate of 0.001 V/s, with an initial potential of -0.42 V vs OCP (open circuit potential) and a final potential of 0.95 V vs OCP. The EIS was taken 120 seconds after immersion to determine the OCP. The OCP determination time was chosen because the average OCP had a stable value with a deviation of less than 5% from t = 0 s to t = 120 s. The stability of the average OCP value indicates that the TiO_2 film on the titanium surface is growing slowly and that the titanium surface is stable. The OCP stability as a function of time in titanium alloys in 3.5% NaCl solution has also been reported [16]. The EIS was performed with a frequency range of 100 kHz - 0.05 Hz and an amplitude of 10 mV about OCP. Nova 1.1 examined the electrochemical parameter.

3. RESULT AND DISCUSSION

3.1 Microstructure and Phase Analysis

Figure 1 shows SEM-EDS (scanning electron microscope-energy dispersive spectroscopy) observation Ti-Cu-Ni-Mn-Zn alloy after sintering

at 880 °C for 3 hours. Ti-20Cu-20Ni-20Mn-20Zn alloy exhibits eutectoid structure clearly seen in Fig. 1(a). The eutectoid structure is most likely due to the high Zn concentration. Figure 1(b) depicts a Ti-13Cu-9Ni-5Mn-5Zn alloy with a -Ti microstructure β-Ti [17].

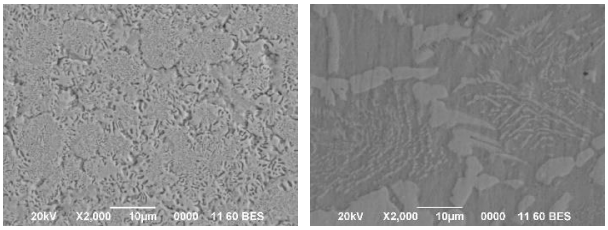

(a) (b)

Figure 1. SEM-EDS image of (a) Ti-20Cu-20Ni-20Mn-20Zn, and (b) Ti-13Cu-9Ni-5Mn-5Zn, after sintering at T = 880 °C for 3 hours

Figure 2 depicts SEM mapping of a high entropy Ti-20Cu-20Ni-20Mn-20Zn alloy. Titanium was found to be uniformly distributed. The Ti-rich matrix contained a uniform distribution of Ni, Mn, and Zn. Meanwhile, in the Ti-rich matrix, Cu was unequally distributed. According to the SEM-EDS mapping profile, Ti forms intermetallic with Ni, Mn, and Zn.

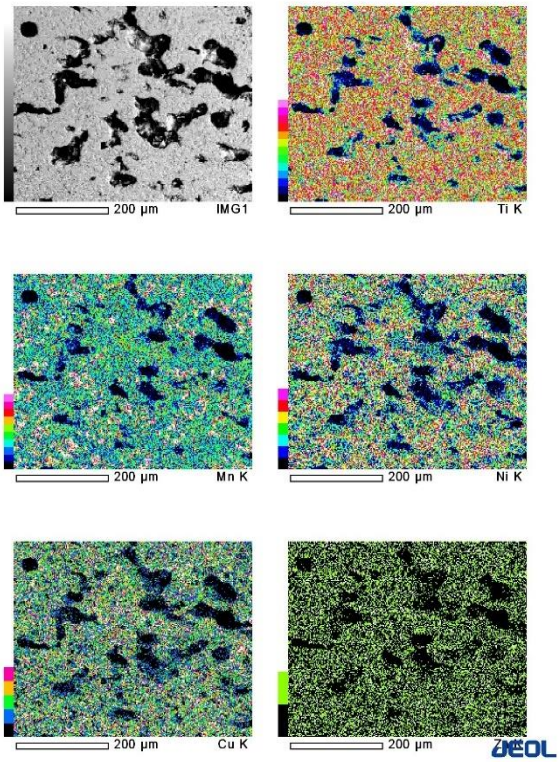

Figure 2. SEM-EDS mapping of Ti-20Cu-20Ni-20Mn-20Zn alloy after sintering at T = 880 °C for 3 hours

Figure 3 depicts SEM mapping of a Ti-13Cu-9Ni-5Mn-5Zn-Ti alloy after 3 hours of sintering at T = 880 °C. The Ti matrix was found to be segregated. Mn and Zn were found in the Ti-rich matrix, but less of Cu and Ni. Cu was observed along grain boundaries. A trace of Ti was discovered in the Cu matrix. Ti tends to form intermetallic with Mn and Zn in the Ti-13Cu-9Ni-5Mn-5Zn alloy, according to the SEM-EDS mapping profile (Fig. 3). Ti-20Cu-20Ni-20Mn-20Zn and Ti-13Cu-9Ni-5Mn-5Zn have distinct microstructures, particularly in terms of Cu phase distribution.

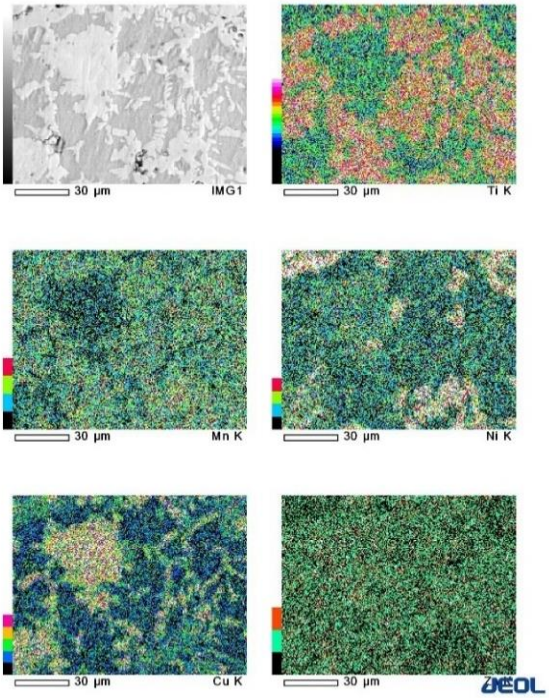

Figure 3. SEM-EDS mapping of Ti-13Cu-9Ni-5Mn-5Zn alloy after sintering at T = 880 °C for 3 hours

Phase analysis of the XRD (x-ray diffraction) results on Ti-20Cu-20Ni-20Mn-20Zn and Ti-13Cu-9Ni-5Mn-5Zn after sintering at a temperature of 880 °C for 3 hours can be seen in Fig. 4. X-ray diffractogram of Ti-20Cu-20Ni-20Mn-20Zn alloy shows the presence of α-Ti, TiNi, Ti_2Ni, $TiZn_2$, $TiMn_2$, and Cu, following the result of phase diagram analysis [14], [18]-[20]. The Cu phase (cubic structure and cell parameters a=b=c=2.561), intermetallic TiNi (hexagonal structure and cell parameters a=4.6460; b=4.1080; c=2.8980), and intermetallic $TiZn_2$ (hexagonal structure and cell parameters a=5.0640; c=8.2100) have the highest intensity in the Ti-20Cu-20Ni-20Mn-20Zn. The second highest intensity (2=44.88°) is found in the intermetallic TiNi phase (hexagonal structure and cell parameters a=4.6460; b=4.1080; c=2.8980) and the intermetallic $TiMn_2$ phase (hexagonal structure and cell parameters a=4.8200; c=7.9150). The third highest intensity is the intermetallic Ti_2Ni phase (2θ=41.57º) with a cubic structure and cell parameters a=b=c= 11.3193. The fourth intensity is the intermetallic

TiNi phase (2θ=41.06º) with a hexagonal structure and cell parameter a=4.6460; b=4.1080; c=2.8980. The fifth intensity (2θ=39.11º) is the α-Ti phase (hexagonal structure and cell parameter a=2.934; b=2.934; c=4.657), intermetallic TiNi (hexagonal structure and cell parameter a=4.6460; b=4.1080; c=2.8980) and intermetallic Ti_2Ni (cubic structure and cell parameters a=b=c=11.3193).

On the other hand, the x-ray diffractogram of Ti-13Cu-9Ni-5Mn-5Zn alloy shows the presence of β-Ti, $TiZn_2$, Ti_3Cu, TiNi, $TiMn_2$, and Cu, by the result of phase diagram analysis as shown at Fig. 3 [14], [18]-[19], [21]. The one dominant peak, namely the intermetallic Ti_3Cu phase, is located at 2θ=39,57º (hexagonal structure and cell parameter a=4.1580; c=3.5940). The second peak is the intermetallic TiNi phase, which is located at 2θ=41.06º (hexagonal structure, and cell parameter a=4.6460; b=4.1080; c=2.8980). The third peak (2θ=38.47º) is the β-Ti phase (cubic structure and cell parameters a=b=c=2.941) and the intermetallic $TiZn_2$ (hexagonal structure and cell parameters a=5.0640; c=8.2100).

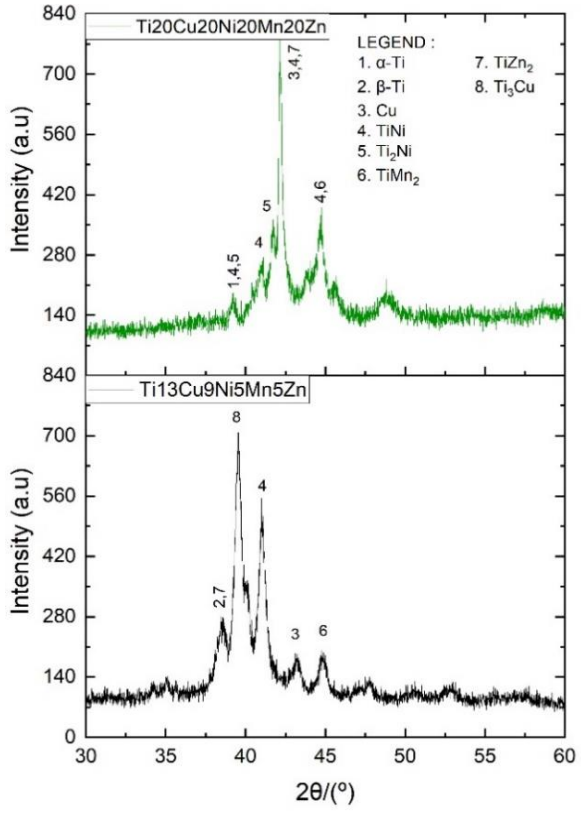

Figure 4. X-ray diffraction pattern of Ti-20Cu-20Ni-20Mn-20Zn and Ti-13Cu-9Ni-5Mn-5Zn alloys after sintered at T= 880 °C for 3 hours

The $TiMn_2$ intermetallic phase is located at 2=44.88° (hexagonal structure, and cell parameters a=4.8200; c=7.9150). The fifth peak, at 2=43.29° (cubic structure and cell parameters a=b=c=2.561), is the Cu elemental phase.

Based on XRD analysis, it is confirmed that α-Ti was formed in Ti-20Cu-20Ni-20Mn-20Zn, while β-Ti was formed in Ti-13Cu-9Ni-5Mn-5Zn. It is well known that α-Ti alloys have low strength properties and are less ductile compared to β-Ti alloys due to the hexagonal closed package structure. β-Ti alloys, which have a BCC (body-centered cubic) structure, tend to have high specific properties, high fatigue, high-temperature, corrosion, and high ductility [2]. Cu elemental phase in the Ti-20Cu-20Ni-20Mn-20Zn high entropy alloy was observed at a higher concentration and intensity than the Ti-13Cu-9Ni-5Mn-5Zn alloy. Based on SEM-EDS mapping and XRD results, it can be seen that the Ti-20Cu-20Ni-20Mn-20Zn and Ti-13Cu-9Ni-5Mn-5Zn alloys have a significant difference in phase concentration and phase distribution of intermetallic titanium and titanium elemental.

3.2 Hardness Result

The hardness value of Ti-20Cu-20Ni-20Mn-20Zn high entropy alloy and Ti-13Cu-9Ni-5Mn-5Zn beta titanium alloy after sintering at a temperature of 880 °C for 3 hours can be seen in Fig. 5. The hardness value of Ti-20Cu-20Ni-20Mn-20Zn was 190.658 HV and Ti-13Cu-9Ni-5Mn-5Zn was 430.736 HV. This could be due to the high intensity of the Cu elemental phase and the low intensity of the α-Ti phase in the Ti-20Cu-20Ni-20Mn-20Zn alloy. The low concentration of the α-Ti phase is likely because titanium tends to form an intermetallic phase with Ni, Mn, and Zn. It's well known that α-Ti has less strength and is brittle [2], and intermetallic Zn exhibit lower hardness than titanium [22]. Contrary to Ti-13Cu-9Ni-5Mn-5Zn alloy, a less intermetallic phase of titanium with Cu, Ni, Mn, and Zn was formed so that a higher β-Ti phase was observed. β-Ti has more strength and ductility [2], [3]. Besides that, Ti-20Cu-20Ni-20Mn-20Zn has more porosity on the surface than Ti-13Cu-9Ni-5Mn-5Zn. The hardness test result confirmed that lower single phase concentration and higher intermetallic phase concentration results in a softer alloy.

A. S. Oryshchenko et al., reported commercial titanium marine with hardness value [1]. The Ti40Al10V alloy reported have hardness value of 250 HV, the Ti6Al4V6Mo alloy reported have hardness value of 60.87 HV, and the Ti3Al8V4Mo4Zr alloy reported have hardness value of 118 HV [23]–[25]. From this comparison, Ti-13Cu-9Ni-5Mn-5Zn is a

promising candidate for marine structure because it has a higher hardness.

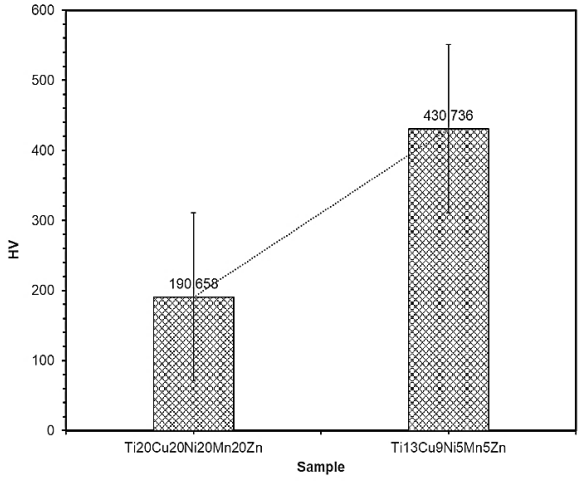

Figure 5. The hardness value comparison between Ti-20Cu-20Ni-20Mn-20Zn and Ti-13Cu-9Ni-5Mn-5Zn after sintered at T= 880 °C for 3 hours

Hence, it is expected to be more resistant to friction and plastic deformation.

3.3 Electrochemical Measurements Analysis

Potentiodynamic polarization was used to determine the corrosion potential and corrosion current density of Ti-Cu-Ni-Mn-Zn alloys in a 3.5% NaCl solution. Figure 6 shows the potentiodynamic polarization results of the two samples in a 3.5% NaCl solution. Both samples showed an active-passive corrosion behavior. Corrosion potential and current density obtained from Tafel extrapolation are presented in Table 1. Ti-13Cu-9Ni-5Mn-5Zn alloy showed a more positive corrosion potential and a lower corrosion current density than that of Ti-20Cu-20Ni-20Mn-20Zn alloy, which indicates that Ti-13Cu-9Ni-5Mn-5Zn alloy is nobler and has better corrosion resistance in a 3.5% NaCl solution compared to Ti-20Cu-20Ni-20Mn-20Zn.

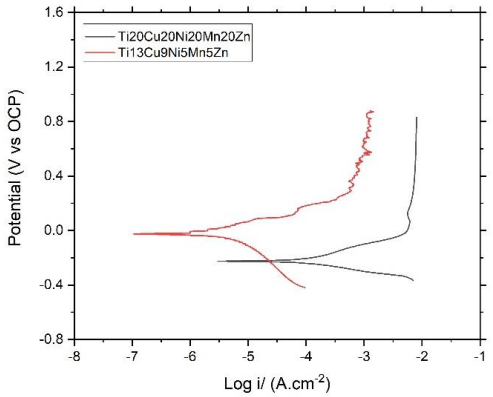

Figure 6. Potentiodynamic polarization of each composition of Ti-Cu-Ni-Mn-Zn alloy after sintered at T= 880 °C for 3 hours

Corrosion rate values of the Ti-20Cu-20Ni-20Mn-20Zn high entropy alloy and the Ti-13Cu-9Ni-5Mn-5Zn alloy calculated from the corrosion current density were 1.799 mm/year and 0.121 mm/year, respectively. That was reported that beta titanium has a stable oxide form [26]. Due to the presence of multiple elements in Ti-20Cu-20Ni-20Mn-20Zn alloy, titanium oxide film tends to be inhomogeneous (non-uniform). The inhomogeneous oxide film in Ti-20Cu-20Ni-20Mn-20Zn alloy is more reactive to Cl^- ion than the titanium oxide film that of Ti-13Cu-9Ni-5Mn-5Zn.

Table 1. Corrosion rate of the Ti-Cu-Ni-Mn-Zn alloy after sintered at T= 880 °C for 3 hours

Samples	E_{corr} (V vs. OCP)	I_{corr} (μA/cm^2)	Corrosion Rate (mm/y)
Ti-20Cu-20Ni-20Mn-20Zn	-0.225	117.130	1.7992
Ti-13Cu-9Ni-5Mn-5Zn	-0.018	7.891	0.1212

Ti-13Cu-9Ni-5Mn-5Zn alloy thermodynamically. However, it must not be that the Ti-13Cu-9Ni-5Mn-5Zn alloy possesses a lower current density compared to the Ti-20Cu-20Ni-20Mn-20Zn alloy. Due to the small current density, kinetically, the tendency of mass loss for pitting formation in Ti-13Cu-9Ni-5Mn-5Zn alloy was very slow. From the above results, it can be concluded that the Ti-13Cu-9Ni-5Mn-5Zn alloy is suitable to be applied as material in a seawater environment [27].

Ti-13Cu-9Ni-5Mn-5Zn and Ti-20Cu-20Ni-20Mn-20Zn alloys exhibit different potentiodynamic polarization curves. The difference in the potentiodynamic polarization curve indicates a difference in corrosion mechanisms in two other alloy surfaces. Based on the potentiodynamic polarization curve, the tendency for pitting formation was observed in Ti13Cu9Ni5Mn5Zn alloy thermodynamically. However, it must be not the Ti13Cu9Ni5Mn5Zn alloy possesses lower current density compared to Ti20Cu20Ni20Mn20Zn alloy. Due to small current density, kinetically, the tendency of mass loss for pitting formation in Ti13Cu9Ni5Mn5Zn alloy was very slow. From the above results, it can be concluded that the Ti13Cu9Ni5Mn5Zn alloy is suitable to be applied as material in a seawater environment.

The EIS (electrochemical impedance spectroscopy) characterization was used to determine phenomena that occuring on the Ti-Cu-Ni-Mn-Zn alloy's surface [28]. The results of the EIS measurements of Ti-20Cu-20Ni-20Mn-

20Zn and Ti-13Cu-9Ni-5Mn-5Zn are presented in Nyquist plots, Bode Modulus plots, and Bode Phase plots in 3.5% NaCl solution, which can be seen in Fig. 7.

The Nyquist plot of both samples immersed in 3.5% NaCl solution showed a similar shape but different in diameter, indicating a difference in the corrosion rate. Nyquist plot of both Ti-20Cu-20Ni-20Mn-20Zn high entropy alloy and Ti-13Cu-9Ni-5Mn-5Zn beta titanium has one semi-circle. The loop is at high to low frequency. The equivalent circuit obtained from the curve fitting consists of the R_s (electrolyte resistance) in series with the CPE (constant phase element) and R_{ct} (charge transfer resistance), as shown in Fig. 8.

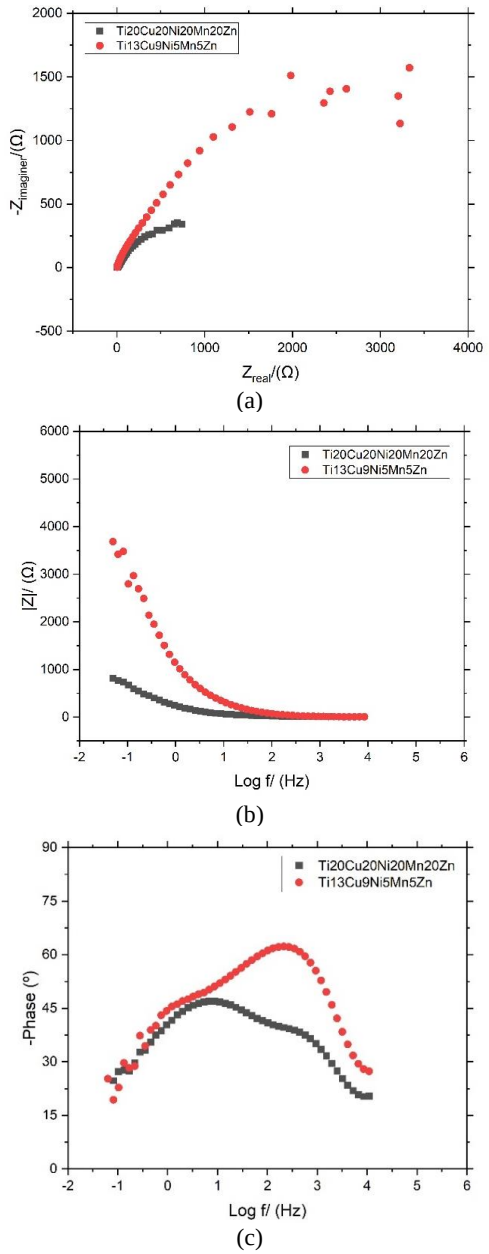

Figure 7. (a) Nyquist plot, (b) Bode modulus, and (c) Bode phase of each composition of Ti-Cu-Ni-Mn-Zn alloy after sintered at T= 880 °C for 3 hours

Figure 8 shows an equivalent circuit model representing the interface characteristics between the porous electrode and the electrolyte [29]. The circuits representing the pore's environment were added in parallel to the equivalent circuit model expressing the geometric electrode surfaces. This equivalent circuit consists of R_s representing the resistance in the electrolyte, R_{ct} representing the charge transfer resistance at the electrode interface, and CPE representing the electrical double layer capacitance at the electrode surface [29]. The interface layer of the Ti-20Cu-20Ni-20Mn-20Zn alloy has more pores than that of Ti-13Cu-9Ni-5Mn-5Zn alloy. This can be seen by a three parallel circuit added in Fig. 8(a), while Fig. 8(b) was only simulated with a two parallel circuit [29].

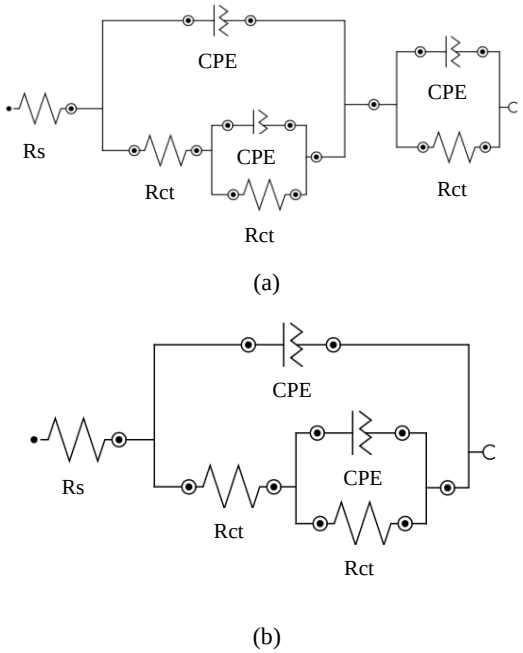

Figure 8. Equivalent circuit (a) Ti-20Cu-20Ni-20Mn-20Zn alloy and (b) Ti-13Cu-9Ni-5Mn-5Zn alloy, after sintered at T= 880 °C for 3 hours

The value of each electrical element is presented in Table 2. The R_p value represents the total resistance of R_s and R_{ct}. The higher R_p value of Ti-13Cu-9Ni-5Mn-5Zn β-Ti alloy indicates that the alloy is more resistant to corrosion in a 3.5% NaCl solution than Ti-20Cu-20Ni-20Mn-20Zn high entropy alloy.

Table 2. The results of fitting Ti-Cu-Ni-Mn-Zn alloy after sintered at T= 880 °C for 3 hours using EIS

Samples	R_p (Ω)	Q_n ($s_n\Omega^{-1}cm^{-2}$)	n
Ti-20Cu-20Ni-20Mn-20Zn	2,672.65	$1.390x10^{6}$	0.704
Ti-13Cu-9Ni-5Mn-5Zn	4,884.04	$0.278x10^{-3}$	1.429

Bode Modulus and Bode Phase plots exhibit a similar trend as the Nyquist plot, as seen in Figs.

7(c) and (d). A higher |Z| value was observed for Ti-13Cu-9Ni-5Mn-5Zn compared to Ti-20Cu-20Ni-20Mn-20Zn, indicating the material's higher corrosion resistance. The shift of the |Z| value in the medium frequency in titanium alloy might be related to the possible appearance of double capacitance at the interface of the material layers.

In the Bode Phase plots, the Ti-20Cu-20Ni-20Mn-20Zn high entropy alloy exhibit a lower phase angle compared than the Ti-13Cu-9Ni-5Mn-5Zn β-Ti alloy. The observed difference in phase angle indicates the difference in the corrosion rate of Ti-20Cu-20Ni-20Mn-20Zn and Ti-13Cu-9Ni-5Mn-5Zn alloy. The higher phase means that the alloy is more resistant to corrosion than the lower phase in the 3.5% NaCl solution.

4. CONCLUSION

The Ti-20Cu-20Ni-20Mn-20Zn and Ti-13Cu-9Ni-5Mn-5Zn alloys were successfully fabricated by the powder metallurgy method. Based on SEM-EDS mapping and XRD results, Ti-20Cu-20Ni-20Mn-20Zn and Ti-13Cu-9Ni-5Mn-5Zn alloys have a significant difference in phase concentration and phase distribution of intermetallic titanium and titanium elemental. The Ti-20Cu-20Ni-20Mn-20Zn alloy as a high entropy alloy has a lower hardness value of 190.658 HV and a higher corrosion rate of 1.7992 mm/year. The Ti-13Cu-9Ni-5Mn-5Zn alloy as a beta titanium alloy has a higher hardness value of 430.736 HV and a lower corrosion rate of 0.1212 mm/year. The results obtained indicate that Ti-13Cu-9Ni-5Mn-5Zn has better corrosion resistance in 3.5% NaCl solution and higher hardness than Ti-20Cu-20Ni-20Mn-20Zn for marine structure application.

ACKNOWLEDGMENT

This work supported Research Center for Metallurgy, The National Research and Innovation Agency (BRIN), Serpong.

REFERENCES

[1] A. S. Oryshchenko, I. V. Gorynin, V. P. Leonov, A. S. Kudryavtsev, V. I. Mikhailov, and E. V. Chudakov, "Marine titanium alloys: Present and future," *Inorg. Mater. Appl. Res.*, vol. 6, no. 6, pp. 571-579, 2015. Doi: 10.1134/S2075113315060106.

[2] F. Rokhmanto, "Pengaruh kandungan Mo dan Nb di dalam paduan logam implan (Ti-Al-Mo dan Ti-Al-Nb) terhadap pembentukan fasa beta," *Universitas Indonesia*, pp. 5-10, 2009.

[3] R. P. Kolli and A. Devaraj, "A review of metastable beta titanium alloys," *Metals (Basel).*, vol. 8, no. 7, pp. 1-41, 2018. Doi: 10.3390/met8070506.

[4] R. W. Schutz, "Environmental behavior of beta titanium alloys," *Jom*, vol. 46, no. 7, pp. 24-29, 1994. Doi: 10.1007/BF03220744.

[5] J. D. Cotton Robert, D. Briggs, Rodney R. Boyer, S. Tamirisakandala, P. Russo, N. Shchetnikov and John C. Fanning, "State of the art in beta titanium alloys for airframe applications," *Jom*, vol. 67, no. 6, pp. 1281–1303, 2015. Doi: 10.1007/s11837-015-1442-4.

[6] M. H. Tsai and J. W. Yeh, "High-entropy alloys: A critical review," *Mater. Res. Lett.*, vol. 2, no. 3, pp. 107–123, 2014. Doi: 10.1080/21663831.2014.912690.

[7] Y. F. Ye, Q. Wang, J. Lu, C. T. Liu, and Y. Yang, "High-entropy alloy: challenges and prospects," *Mater. Today*, vol. 19, no. 6, pp. 349–362, 2016. Doi: 10.1016/j.mattod.2015.11.026.

[8] E. P. George, D. Raabe, and R. O. Ritchie, "High-entropy alloys," *Nat. Rev. Mater.*, vol. 4, no. 8, pp. 515–534, 2019. Doi: 10.1038/s41578-019-0121-4.

[9] A. Sasongko, J. Setiawan, H. Hardiyanti, R. Suryadi, T. Yulianto and R. Langenati, "Perhitungan komposisi paduan high-entropy alloy AlCrMoNbZr untuk karakterisasi bahan struktur elemen bakar reaktor daya," *Hasil-Hasil Penelitian EBN Tahun 2020, BRIN Nuclear Energy Research Organization*, October, 2021. Doi: 10.13140/RG.2.2.21176.26885.

[10] J. Yeh, Y. Chen, S. Lin, and S. Chen, "High-entropy alloys – A new era of exploitation," *Materials Science Forum.*, vol. 560, pp. 1-9, 2007. Doi: 10.4028/www.scientific.net/MSF.560.1.

[11] D. B. Miracle and O. N. Senkov, "A critical review of high entropy alloys and related concepts," *Acta Mater.*, vol. 122, pp. 448–511, 2017. Doi: 10.1016/j.actamat.2016.08.081.

[12] Y. F. Ye, Q. Wang, J. Lu, C. T. Liu, and Y. Yang, "High-entropy alloy : challenges and prospects," *Materials Science*, vol. 00, no. 00, 2015. Doi: 10.1016/j.mattod.2015.11.026.

[13] N. Ma, S. Liu, W. Liu, L. Xie, D. Wei, L. Wang, L. Li, B. Zhao, Y. Wang , "Research progress of titanium-based high entropy alloy: Methods, properties,

and applications," *Front. Bioeng. Biotechnol*., vol. 8, no. November, pp. 1-18, 2020. Doi: 10.3389/fbioe.2020.603522.

[14] G. P. Vassilev, X. J. Liu, and K. Ishida, "Reaction kinetics and phase diagram studies in the Ti-Zn system," *J. Alloys Compd.*, vol. 375, no. 1-2, pp. 162-170, 2004. Doi: 10.1016/j.jallcom.2003.11.026.

[15] M. J. Mindel and S.R. Pollack, "The room temperature oxidation," *Acta Metall.*, vol. 17, p. 1441, 1969.

[16] S. Pan and W. Tsai, "Polarity reversal of titanium-coupled brass in 3.5 wt % NaCl solution Polarity reversal of titanium-coupled brass in 3.5 wt % NaCl solution Kadek Trisna Surya Hariyantha Szu-Jung Pan," *Conference: The International Corrosion Prevention Symposium for Research Scholars (CORSYM-2014) at Bombay, India*, 2014. Doi: 10.13140/2.1.2324.1609.

[17] M. J. Donachie, *Titanium - A Techincal Guide*, vol. 99, no. 5. 2000. [Online]. Available: http://www.intechopen.com/books/corrosion-resistance. Date of access: 20 February 2022.

[18] M. Kikuchi, Y. Takada, S. Kiyosue, M. Yoda, M. Woldu, Z. Cai, O. Okuno, T. Okabe, "Mechanical properties and microstructures of cast Ti-Cu alloys," *Dent. Mater.*, vol. 19, no. 3, pp. 174-181, 2003. Doi: 10.1016/S0109-5641(02)00027-1.

[19] T. Nakahata, "Industrial processing of titanium–nickel (Ti–Ni) shape memory alloys (SMAs) to achieve key properties", *Woodhead Publishing Limited*, pp. 53-62, 2011. Doi: 10.1533/9780857092625.1.53.

[20] J. L. Murray, "The Mn-Ti (Manganese-Titanium) system," *Bulletin of Alloy Phase Diagrams*, vol. 2, no. 3, pp. 334-343, 1981.

[21] Y. Alshammari, F. Yang, and L. Bolzoni, "Mechanical properties and microstructure of Ti-Mn alloys produced via powder metallurgy for biomedical applications," *J. Mech. Behav. Biomed. Mater.*, vol. 91, pp. 391-397, 2019. Doi: 10.1016/j.jmbbm.2018.12.005.

[22] H. Okamoto, "Ti-Zn (Titanium-Zinc)," *J. Phase Equilibria Diffus.*, vol. 29, no. 2, pp. 211-212, 2008. Doi: 10.1007/s11669-008-9271-6.

[23] Y. Yuan, Y. Wu, Z. Yang, X. Liang, Z. Lei, H. Huang, H. Wang, X. Liu, K. An, W. Wu and Z. Lu, "Formation, structure and properties of biocompatible TiZrHfNbTa high-entropy alloys," *Mater. Res. Lett.*, vol. 7, no. 6, pp. 225-231, 2019. Doi: 10.1080/21663831.2019.1584592.

[24] D. Wu, W. lin Wang, L. gang Zhang, Z. yu Wang, K. chao Zhou, and L. bin Liu, "New high-strength Ti–Al–V–Mo alloy: from high-throughput composition design to mechanical properties," *Int. J. Miner. Metall. Mater.*, vol. 26, no. 9, pp. 1151-1165, 2019. Doi: 10.1007/s12613-019-1854-1.

[25] A. Abada, S. Bergheul, and A. Younes, "Mechanical and structural behaviour of TiAlV nanocrystalline elaborated by mechanical milling technique," *Micro Nano Lett.*, vol. 15, no. 14, pp. 1023-1027, 2020. Doi: 10.1049/mnl.2020.0336.

[26] D. Prando, A. Brenna, M. V. Diamanti, S. Beretta, F. Bolzoni, M. Ormellese and M. Pedeferri, "Corrosion of titanium: Part 2: Effects of surface treatments," *J. Appl. Biomater. Funct. Mater.*, vol. 16, no. 1, pp. 3-13, 2018. Doi: 10.5301/jabfm.5000396.

[27] Z. Yan, X. Yuan, Z. Tan, M. Tang, and Z. Feng, "Effect of in situ ion nitride treatment on the corrosion behavior of titanium," *Corrosion Science*, vol. 13, pp. 353-361, 2018. Doi: 10.20964/2018.01.23.

[28] S. Feliu, "Electrochemical impedance spectroscopy for the measurement of the corrosion rate of magnesium alloys: Brief review and challenges," *Metals (Basel).*, vol. 10, no. 6, pp. 1-23, 2020. Doi: 10.3390/met10060775.

[29] S. Nomura, H. Tashiro, Y. Terasawa, Y. Nakano, M. Haruta, K. Sasagawa, H. Takehara and J. Ohta, "Randles circuit model for characterizing a porous stimulating electrode of the retinal prosthesis," *Electron. Commun. Japan*, vol. 104, no. 3, pp. 1-9, 2021. Doi: 10.1002/ecj.12324.